

Fabrication and mechanical properties of binderless-WC and WC-CNT hard materials by pulsed current activated sintering Method

Jun-Ho Jang^{a,b}, Ik-Hyun Oh^a, Jae-Won Lim^b and Hyun-Kuk Park^{a,*}

^aKorea Institute of Industrial Technology (KITECH), 1110-9 Oryong-dong, Buk-gu, Gwang-ju, Korea

^bDivision of Advanced Materials Engineering Chonbuk National University, Korea

Using the spark plasma sintering process, WC and WC-5, 10, 15 vol.%CNT hard materials were densified using ultra-fine WC and CNT powders. For the preparing the WC-x vol.%CNT mixed powders, First, the carbon nanotubes were dispersed in N, N-dimethylformamide (DMF) for 30 ~ 90 min using an ultrasonic shaker. WC powder was then added to the nanotube and the mixtures were dispersed ultrasonically for 30 min. Finally, the mixed powders were horizontal ball milled at 250 rpm for 4 hrs in DMF. The WC- vol.%CNT were almost completely dense with a relative density of up to 99% after the simultaneous application of 60 MPa of pressure and about 27 min of electric current without significant change in the grain size. The average grain size of WC, WC-5, 10, and 15 vol.% CNT hard materials were about 327, 348, 306, 302 nm. The compositional and microstructural analyses of the products were carried out through XRD and FE-SEM. The hardness and fracture toughness of the dense WC and WC-x vol.%CNT composites were also investigated.

Key words: WC-CNT, Spark plasma sintering process, Mechanical property, Hard materials, Rapid sintering.

Introduction

Carbon nanotubes (CNTs) are considered to be the best of all nanomaterials. Compared with all types of natural materials, CNTs have the highest theory strength, which are more than 100 times that of steel. Tests have been conducted on CNTs for reinforcing various ceramics, cermets, metals, and alloys because they have many unique mechanical and physical properties [1-7].

Cemented carbides are widely used in various applications for components that wear, i.e., face seals, tools for metal cutting, and rock drilling. Binderless carbides have been developed as a complement to conventional cemented carbides for use in corrosive environments where the metal binder degrades [8]. Normally, binderless carbides have a lower abrasion resistance than metal-rich cemented carbides; however, they have a higher abrasion resistance than that of common engineering ceramics. The main advantages of binderless carbide materials over other ceramics in wear applications is their ability to withstand high pressure and speed in sliding contact without microfracturing [9]. When conventional sintering processes are used to sinter nano-sized powders, concomitant grain growth leads to the destruction of the nanostructure. Attention has therefore been focused on consolidation methods in

which grain growth can be eliminated or significantly reduced. Rapid sintering methods have thus been widely used to sinter nano-sized powders. The most obvious advantage of rapid sintering is that fast heating and cooling rates, as well as short dwell times, lead to the bypassing of low-temperature and non-densifying mass transport (e.g., surface diffusion) [10, 11]. However, conventional rapid heating can lead to temperature gradients and thus differential densification (non-uniform microstructures), low density, or specimen cracking. To overcome these difficulties, other rapid sintering techniques, such as high-frequency induction heated sintering (HFIHS) [12-14] have been developed.

Therefore, controlling the grain growth during sintering is a key component to the commercial success of nanostructured WC-CNT composites. In this study, WC and WC-CNT were sintered using a rapid sintering process known as spark plasma sintering. This method combines a pulsed current with the application of high pressure. The goal of this study was to produce dense, ultra-fine WC and WC-CNT hard materials at very short sintering times (< 27 minutes). Additionally, the mechanical properties of the WC hard materials were investigated.

Experimental Procedure

In this study, 99.95% pure tungsten carbide (0.4 ~ 0.5 μm , TaeguTec Ltd., Korea) and 96% pure MWCNT (diameter 10 ~ 15 nm, length ~ 20 μm (CM95), Han-hwa nanotech Ltd., Korea) powders were used as the starting materials. Figs. 1 and 2 show the field-

*Corresponding author:
Tel : +82-62-600-6181
Fax: +82-62-600-6149
E-mail: hk-park@kitech.re.kr

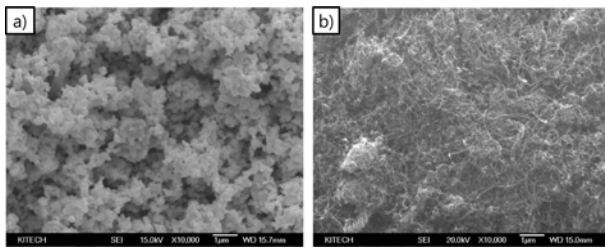


Fig. 1. FE-SEM images of the raw materials; (a) WC and (b) CNT.

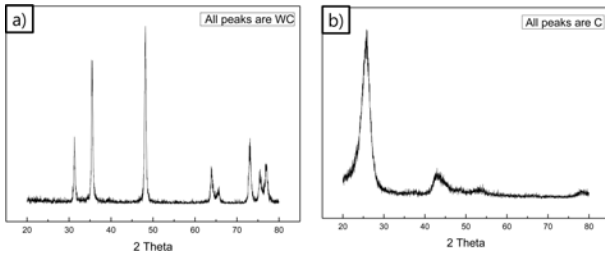


Fig. 2. XRD patterns of raw materials; (a) WC and (b) CNT.

emission scanning electron microscopy (FE-SEM) images and X-ray diffraction (XRD) patterns of the raw materials used. First, the carbon nanotubes were dispersed in N, N-dimethylformamide (DMF) for 30 ~ 90 min using an ultrasonic shaker. WC powder was then added to the nanotube and the mixtures were dispersed ultrasonically for 30 min. Finally, the mixed powders were horizontal ball milled at 250 rpm for 4 hrs in DMF. Zirconia balls (6 mm in diameter) were used in a sealed cylindrical plastic vial. The mixed powders were dried at 120 °C in a vacuum dry oven. For this study, 5, 10, and 15 vol% CNT were mixed with WC powder. Fig. 3 shows the CNT powders after dispersal at various ultrasonic times. Fig. 4 shows the FE-SEM image and XRD pattern of the WC and CNT mixed powders. After milling, the mixed powders were placed in a graphite die (outside diameter, 30 mm; inside diameter, 10 mm; height, 40 mm), and then placed into a spark plasma sintering system (Sumitomo Coal Mining, Japan). A schematic diagram of this method is shown in Fig. 5. The SPS apparatus included a 25 V, 1000 A DC power supply (which provided a pulsed current for 12 ms with an off time of 2 ms through the sample and die), and a 10 ton uniaxial press. First, the system was evacuated, and a uniaxial pressure

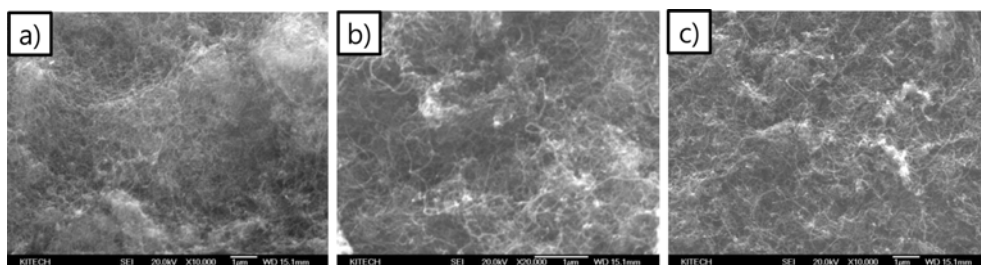


Fig. 3. FE-SEM images of dispersed CNT for different ultrasonic shaker time; (a) 30min, (b) 60min and (c) 90min.

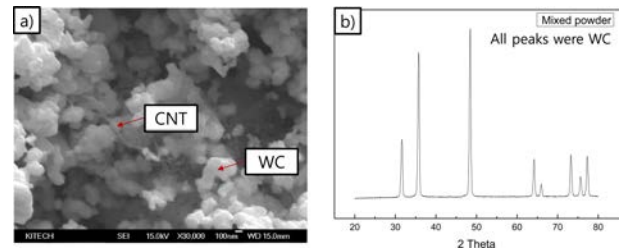


Fig. 4. (a) FE-SEM image and (b) XRD pattern of WC-CNT ball milled powder.

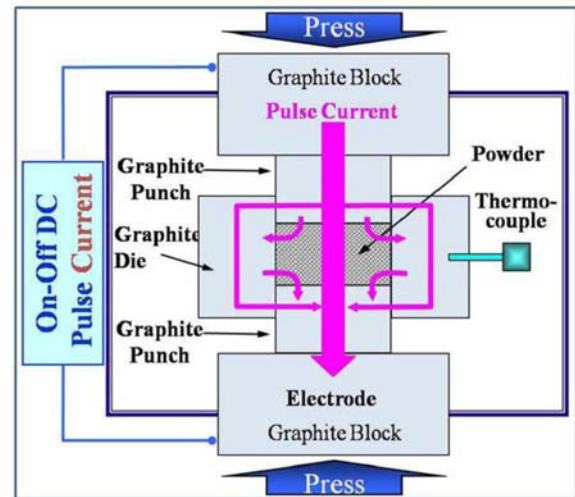


Fig. 5. Schematic diagram of apparatus for SPS.

of 60 MPa was applied. A DC current was then activated and maintained until the densification rate was negligible, as indicated by the observed shrinkage of the sample. The sample shrinkage was measured in real time using a linear gauge for the vertical displacement. The temperature was measured using a pyrometer that was focused on the surface of the graphite die. Depending on the heating rate, the electrical and thermal conductivities of the compact (and its relative density) as well as the temperature on the surface and in the center of the sample could differ. The heating rate was approximately 60 °C/min during this process. After the process was complete, the current was turned off, and the sample was allowed to cool to room temperature. The entire densification process using the SPS technique consisted of four major control stages,

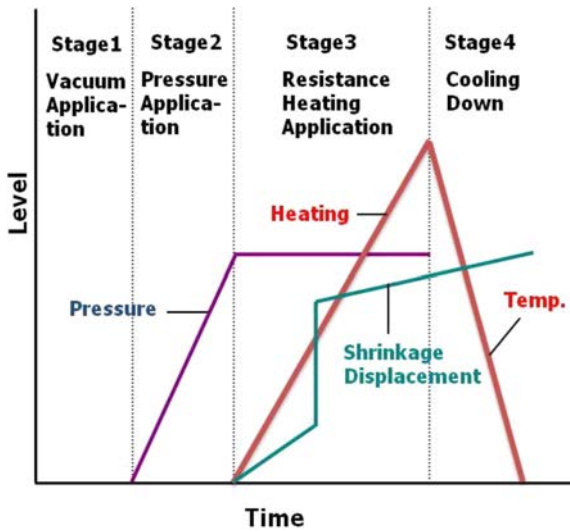


Fig. 6. Schematic representation of the temperature, pressure and shrinkage displacement profile during SPS.

including chamber evacuation, pressure application, power application, and cool down. The four major sintering stages are schematically shown in Fig. 6. This densification process was carried out under a vacuum of 6 Pa. The relative densities of the sintered samples were measured using the Archimedes method. Microstructural information was obtained from the product samples, which were polished and etched using a Murakami's reagent (5 g $Fe_3(CN)_6$, 5 g NaOH, and 50 ml distilled water) for 60 to 150 sec at room temperature. The compositional and microstructural analyses of the products were carried out through XRD and FE-SEM. The Vickers hardness was measured by performing indentation tests at a load of 30 kg and a dwell time of 15 sec. The carbide grain size, d_{wc} , was obtained using the linear intercept method [15, 16].

Results and Discussion

The variations of shrinkage displacement and temperature with heating during the sintering of WC-x vol.% CNT hard materials using SPS under a pressure of 60 MPa are shown in Fig. 7. When an electric current is applied, the shrinkage displacement is nearly constant at up to 870 °C and then abruptly increases at above that temperature. When the temperature reaches about 1600 °C, the densification rate becomes nearly negligible, and the samples densify to the almost theoretical density of about 1770 sec, as will be further discussed below. The sintered relative densities of the WC, WC-3, WC-5, and WC-15vol% CNT samples were 99, 99.4, 98.5, and 98.3%, respectively. The measurements for the shrinkage displacement and the initial height of the powder compact (Fig. 7) were used to measure the height variation of the powdered compact with relative precision as $\Delta L = L_T - L_0 < 0$, where L_T is the instantaneous height and

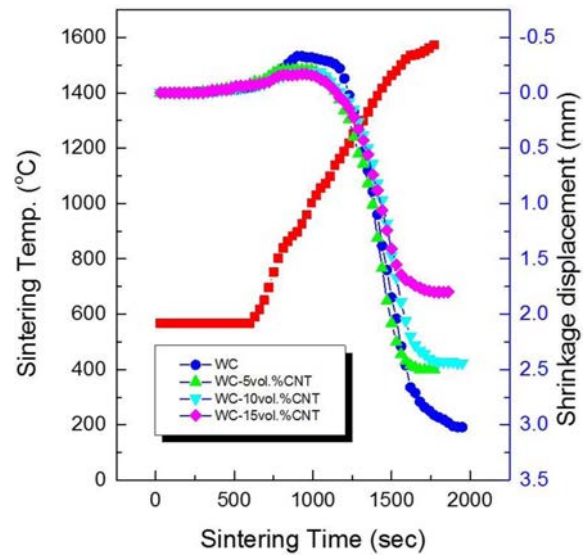


Fig. 7. Variations of temperature and shrinkage displacement with sintering time during SPS of WC-x vol.% CNT hard materials.

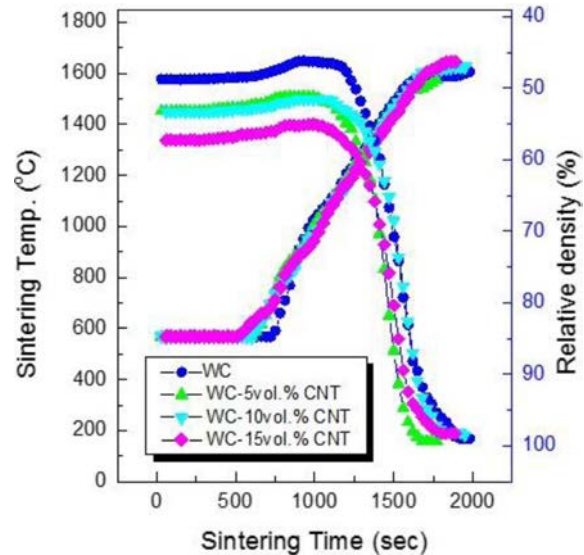


Fig. 8. Variations of temperature and relative density with sintering time during SPS of WC-x vol.% CNT hard materials.

L_0 is the initial height of the powder compact. Therefore, the instantaneous relative density D can be computed as [17]

$$D_T = (L_f / L_T)D_f \tag{1}$$

where D_T is the instantaneous relative density, L_f is the final height, L_T is the instantaneous height, and D_f is the final relative density. Fig. 8 shows the variations in the temperature and the relative density of the WC-x vol.%CNT hard materials with respect to heating time during sintering via SPS at 60 MPa. The relative densities were dependent on the load added to the initial mold, but the relative density changed at about 1100 °C, and then abruptly increased as the temperature

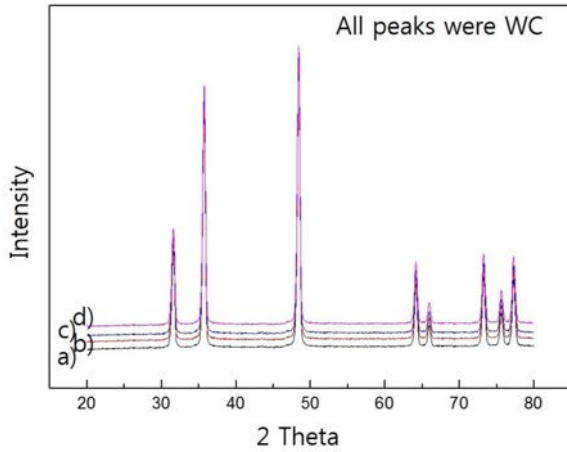


Fig. 9. XRD patterns of WC-x vol.% CNT hard materials; (a) WC, (b) WC-5vol.% CNT, (c) WC-10 vol.% CNT and (d) WC-15 vol.% CNT.

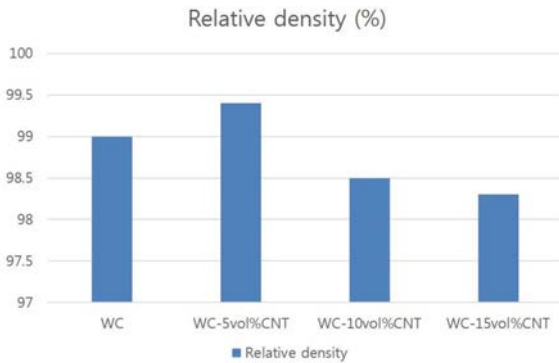


Fig. 10. Relative density of WC-x vol.% CNT hard materials.

increased further. When the temperature reached about 1600 °C, the relative density was almost at a maximum for the WC and WC-x vol.%CNT hard materials.

These results are attributed to two causes. First, because high Joule heating occurs at the point of contact between particles due to an induced current, the spread of atoms is accelerated. In addition, it is considered to be easier to perform sintering at a low temperature because the spread of atoms is accelerated in an electric field. Second, when pressure is applied during sintering, the driving force of the sintering is increased; eq. (1) shows the increased driving force, F_D [18],

$$F_D = \gamma + (P_a r / \pi) \tag{2}$$

where γ is the interfacial energy, and P_a and r are the applied pressure and radius of particle, respectively. Consequently, these results suggest that the most obvious advantages of the SPS process compared with conventional sintering processes are faster heating rates, shorter processing times, and relatively lower temperatures during sintering, allowing for the limitation of grain growth and clean grain boundaries [11, 15].

Fig. 9 shows the XRD patterns of WC and WC-x

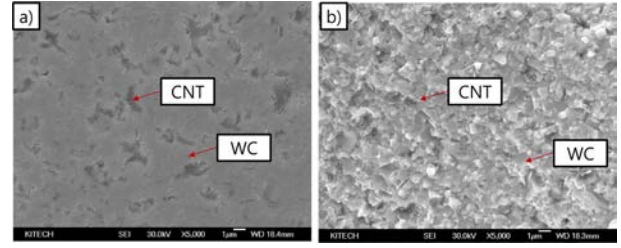


Fig. 11. FE-SEM images of WC-15 vol.% CNT hard materials; (a) etched surface and (b) fracture surface.

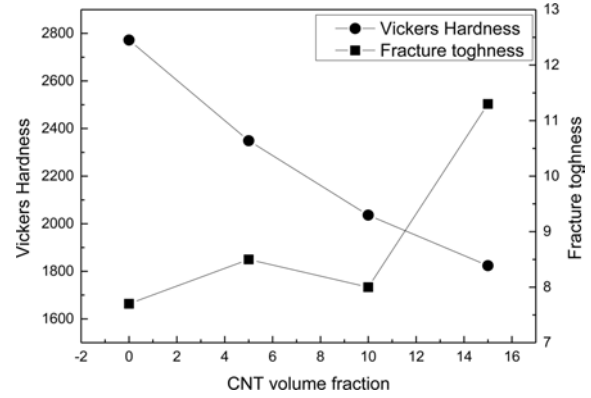


Fig. 12. Vickers hardness and fracture toughness of WC-x vol.% CNT hard materials.

vol.% CNT hard materials after sintering by SPS in this work. For the WC and WC-x vol% CNT hard materials, for pure WC, only peaks belonging to WC were observed, indicating that no compositional changes occurred during sintering. No peaks for the sub-carbide W_2C or any impurity phase were present in Fig. 9.

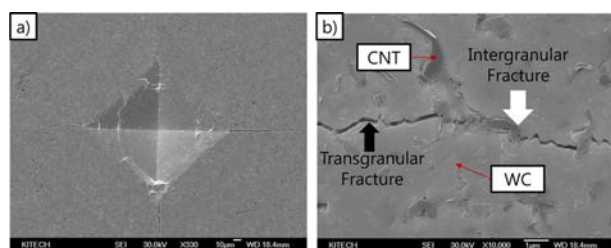
The grain size and the internal strain were calculated using the Stokes and Wilson’s formula [19];

$$b = b_d + b_e = k\lambda / (d\cos\theta) + 4\epsilon\tan\theta \tag{3}$$

where b is the full width at half-maximum (FWHM) of the diffraction peak after the instrumental correction; b_d and b_e are the FWHM for a small grain size and internal strain, respectively; k is a constant (with a value of 0.9); λ is the wavelength of the X-ray radiation; d and ϵ are the grain size and the internal strain, respectively; and θ is the Bragg angle. The parameters b and b_s follow Cauchy’s form with the relationship: $B_0 = b + b_s$, where B_0 and b_s are the FWHM of the broadened Bragg peaks and a standard sample’s Bragg peaks, respectively. The average grain sizes of WC were about 327, 348, 306, and 302 nm for the sintered WC, WC-5, WC-10, and WC-15 vol% CNT hard materials. However, the grain of WC in sintered WC, WC-5, WC-10 and WC-15 vol% CNT showed a fine structure obtained without any grain growth during sintering using the SPS method. Fig. 10 shows the relative density of WC and WC-x vol%CNT hard materials. The WC and WC-x vol%CNT hard materials were almost completely

Table 1. Comparison of mechanical properties of WC-x vol.% CNT sintered in this study with previously reported values.

Ref.	Binder contents (wt.%)	Relative density (%)	Grain size (μm)	HV (Kg/mm^2)	KIC ($\text{MPa}\cdot\text{m}^{1/2}$)
[14]	6Mo2C	99	0.45	2461	4.8
[19]	10Ni	97.5	0.3	1810	13.5
[22]	9Co	99.4	0.26	1992	11.9
[23]	10Co	99.5	1.9	1333	13.5
This study	WC	99	0.327	2772	7.7
	WC-5 vol.%CNT	99.4	0.348	2348	8.5
	WC-10 vol.%CNT	98.5	0.306	2036.1	8
	WC-15 vol.%CNT	98.3	0.302	1823.9	11.3

**Fig. 13.** (a) Vickers hardness indentation and (b) median crack propagation of the sintered WC-15 vol.% CNT.

dense with a relative density of up to 99%. Fig. 11 shows the FE-SEM images of the etched surface and fracture surface of the WC-15 vol% CNT hard material, which was 1600 °C at a pressure of 60 MPa.

The Vickers hardness measurements were taken on the polished sections of the WC and WC-x vol%CNT hard materials using a 30 kgf load at a dwell time of 15 s. At sufficiently large loads, the indentations produced median cracks that emanated from the corners of the indent. The fracture toughness was calculated from the cracks that were produced from the indentations under large loads. The length of these cracks permits an estimation of the fracture toughness of the materials by the expression [20]:

$$K_{IC} = 0.204(c/a)^{-3/2} H_v a^{1/2} \quad (4)$$

where c is the trace length of the crack measured from the center of the indentation, a is half of the average length of two indent diagonals, and H_v is the hardness. As for the hardness values, the toughness values were derived from the average of five measurements. The calculated Vickers hardness and fracture toughness values of the WC and WC-x vol%CNT hard materials are shown in Fig. 12. Table 1 shows the calculated structural characteristics of the WC and WC-x vol.% CNT hard materials, including the hardness and

fracture toughness values from the above formulas based on the planar section measurements.

A typical indentation pattern for the WC-15 vol.% CNT hard material is shown in Fig. 13(a). Typically, one to three additional cracks propagated from the indentation corner. A higher magnification view of the indentation median crack in the composite is shown in Fig. 13(b). This figure shows that the crack propagated along the phase boundary of WC and CNT. The crack segments ran both along the WC-CNT phase boundaries (white arrows) and through the WC phase itself (black arrows). The CNT binder phase is known to prevent crack propagation in the cemented carbide by shielding a stress field in front of the crack tip or by bridging the crack forming ligaments behind the crack tip [13, 20-24].

Summary

WC-xvol.% CNT hard materials were rapidly consolidated using the spark plasma sintering method with ultra-fine WC and dispersed CNT powders. Almost fully dense WC-xvol.% CNT was obtained within 27 min. The grain sizes of WC, WC-5, WC-10, and WC-15 vol.% CNT were about 327, 348, 306, 302 nm, respectively, and the nano-structure was obtained without any grain growth during sintering using the SPS method. The fracture toughness values of WC, WC-5, WC-10, and WC-15 vol.% CNT were 7.7 $\text{MPa}\cdot\text{m}^{1/2}$, 8.5 $\text{MPa}\cdot\text{m}^{1/2}$, 8.0 $\text{MPa}\cdot\text{m}^{1/2}$, and 11.3 $\text{MPa}\cdot\text{m}^{1/2}$, respectively, and the Vickers hardness values of WC, WC-5, WC-10, and WC-15 vol.% CNT were 2772 kg/mm^2 , 2348 kg/mm^2 , 2036.1 kg/mm^2 , and 1823.9 kg/mm^2 , respectively, at 60 MPa and 1600 °C.

Acknowledgments

This study has been conducted with the support of the Korea Institute of Industrial Technology as "Source technology development project, EO-17-0015".

References

1. Y.Q. Liu, L. Gao, Carbon 43 (2005) 47-52.
2. Z. Xia, L. Riester, W.A. Curtim, H. Li, B.W. Sheldon, J. Lian, B. Chang, J.M. Xu, Acta Mater. 52 (2004) 931-944.
3. J.W. Ning, J.J. Zhang, Y.B. Pan, J.K. Guo, Mater. Sci. Eng. A 357 (2003) 392-396.
4. S.I. Cha, K.T. Kim, K.H. Lee, C.B. Mo, S.H. Hong, Scripta Mater. 53 (2005) 793-797.
5. E. Flahaut, A. Peigney, Ch. Laurent, Ch. Marliere, F. Chastel, A. Rousset, Acta Mater. 48 (2000) 3803-3812.
6. Ch. Laurent, A. Peigney, O. Dumortier, A. Rousset, J. Eur. Ceram. Soc. 18 (1998) 2005-2013.
7. X.H. Chem, C.S. Chen, H.N. Xiao, H.B. Liu, L.P. Zhou, S.L. Li, G. Zhang, Tribol. Int. 39 (2006) 22-28.
8. S. Imasato, K. Tokumoto, T. Kitada, S. Kakaguchi, Int. Refract. Met. Hard Mater. 13 (1995) 305-312.
9. H. Engqvist, N. Axen, S. Hogmark, Tribol. Lett. 4 (1998) 251-258.

10. M.P. Harmer, R.J. Brook, *J. Br. Ceram. Soc.* 80 (1981) 147-149.
11. A. Morell, A. Mermosin, *Bull. Am. Ceram. Soc.* 59 (1980) 626-629.
12. H.C. Kim, I.J. Shon, Z.A. Munir, *J. Mater. Sci.* 40 (2005) 2849-2854.
13. H.C. Kim, D.Y. Oh, I.J. Shon, *Int. J. Ref. Met. Hard Mater.* 22 (2004) 197-203.
14. H.C. Kim, H.K. Park, I.K. Jung, I.Y. Ko, I.J. Shon, *Ceramics Int.* 34 (2008) 1419-1423.
15. K. Jia, T.E. Fischer, G. Gallois, *Nanostruct Mater.* 10 (1998) 875-891.
16. J.H. Han, D.Y. Kim, *Acta Mater.* 46 (1998) 2021-2028.
17. Bernard-Granger M., Huizard C., *J. Acta Mater.* 55(10) (2007) 3493-3504.
18. H.K. Park, J.H. Ryu, H.J. Youn, J.M. Yang, I.H. Oh, *Mater. Trans.* 53 (2012) 1056-1061.
19. F.L. Zhang, C.Y. Wang, M. Zhu, *Scripta Mater.* 49 (2003) 1123-1128.
20. N. Koichi, *J. Mater. Sci. Lett.* 1 (1982) 12-16.
21. L.S. Sigl, H.F. Fischmeister, *Acta Metall.* 36 (1988) 887-897.
22. L.S. Sigl, P.A. Mataga, B.J. Dalgleish, R.M. McMeeking, A.G. Evans, *Acta Metall.* 36 (1988) 945-958.
23. H.C. Kim, D.Y. Oh, I.J. Shon, *Int. J. Ref. Met. Hard Mater.* 22 (2004) 197-203.
24. S. Imasato, K. Tokumoto, T. Kitada, S. Sakaguchi, *Inter. J. of Ref. Met. & Hard Mater.* 13 (1997) 305-312.